A Compton scattering image reconstruction algorithm based on total variation minimization*

Li Shou-Peng(李守鹏), Wang Lin-Yuan(王林元), Yan Bin(闫 镔)†, Li Lei(李 磊), and Liu Yong-Jun(刘拥军)

National Digital Switching System Engineering & Technology Research Center, Zhengzhou 450002, *China*

(Received 29 February 2012; revised manuscript received 9 April 2012)

Compton scattering imaging is a novel radiation imaging method using scattered photons. Its main characteristics are detectors that do not have to be on the opposite side of the source, so avoiding the rotation process. The reconstruction problem of Compton scattering imaging is the inverse problem to solve electron densities from nonlinear equations, which is ill-posed. This means the solution exhibits instability and sensitivity to noise or erroneous measurements. Using the theory for reconstruction of sparse images, a reconstruction algorithm based on total variation minimization is proposed. The reconstruction problem is described as an optimization problem with nonlinear data-consistency constraint. The simulated results show that the proposed algorithm could reduce reconstruction error and improve image quality, especially when there are not enough measurements.

Keywords: Compton scattering tomography, inverse problem, image reconstruction, sparse, total variation

PACS: 87.57.nf, 83.85.Hf, 06.30.Dr **DOI:** 10.1088/1674-1056/21/10/108703

1. Introduction

Radiation imaging technology has been widely used in industrial, medical, and many other fields. It traditionally uses transmitting photons, such as in radiography and computed tomography (CT).[1,2] A novel radiation imaging method using scattered photons is Compton scattering imaging, which was proposed by Lale[3] and developed by a number of researchers.[4,5] The main characteristics of Compton scattering imaging are that detectors do not have to be on the opposite side of the source and so there is no rotation process. Thus Compton scattering tomography allows massive objects and one side accessible objects to be imaged. This technique can be used in historical exploration,[6] nondestructive testing,[7] landmine detection,[8] human head imaging,[9] mammographic screening,[10,11] and so on.

Lale, the pioneer of Compton scattering imaging, regarded radiation attenuation as being negligible because he used a high energy beam. Battista and Bronskill[4] proposed a pixel-by-pixel rectilinear scanning approach, which allowed for progressive correction for attenuation by the previously evaluated densities of the foregoing pixel along the incident beam. However the error of the previously evaluated densities will affect the following densities.

Farmer and Collins *et al.*[5] utilized the famous Compton scattering kinematics equation relating to the energy and angle of single scattered photons to fix on the scattered position. They used a pencil beam collimator and measured the energy spectrum of the scattered photons with a wide-angle collimated germanium detector. A new model using a fan beam collimator was proposed by Kondic *et al.*[12] The attenuation coefficients of the incident beam and scattered beam are considered as unknown quantities, together with the unknown electron densities, then a linear problem with $3N^2$ unknowns was formulated. Hussein *et al.*[13] dealt with this problem as a nonlinear problem with N^2 unknowns.[13]

In Compton scattering image reconstruction, the number of independent measurements is usually not equal to the number of unknown densities. The images reconstruction problem is ill-posed, so a solution is sensitive to noise or erroneous measurements. The common way to deal with an ill-posed problem is regularization techniques, which make a compromise between the maximum fidelity to the measurements and

*Project supported by the National Basic Research Program of China (Grant No. 2011CB707701) and the National High Technology Research and Development Program of China (Grant Nos. 2009AA012200 and 2012AA011603).

†Corresponding author. E-mail: tom.yan@gmail.com

© 2012 Chinese Physical Society and IOP Publishing Ltd

some prior knowledge about the solution.[14] There is a whole theory of regularization methods in the literature to deal with such problems. The most common methods used in Compton scattering image reconstruction are truncated singular value decomposition (TSVD), Tikhonov–Miller (TM) type of regularization, and a probabilistic expectation maximization-maximum likelihood (EM-ML) method.[15]

Recently Candes *et al.*[16] developed a novel algorithm for the exact recovery of an image from sparse samples of its discrete Fourier Transform (DFT).[16] The exact recovery depends on the fact that there exists some representation of the image which provides sparse coefficients. Medical images often vary rapidly only at the boundaries of internal organs, so images themselves are not sparse but their gradient is usually sparse.[17,18] Such a representation of an image is to minimize the l_1 norm of the image gradient magnitude, namely the total variation (TV) of the image. Sidky and Pan[19] proposed an image reconstruction method by constraining the total variation minimization in CT, and it has turned out that their method can reconstruct the image exactly using fewer measurements. This reconstruction method based on TV minimization was widely studied.[20–24]

2. Forward model of Compton scattering imaging

A schematic plot of the Compton scattering imaging system model is provided in Fig. 1. A fan beam monoenergetic ray is used for irradiating the entire object. Suppose that the energy of photons is E_0 and the source emits N_0 photons at point $\boldsymbol{A}$. Photons scatter within the object, and the the scattered photons are then collected with a high-purity germanium (HPGe) detector at $\boldsymbol{C}$. Considering the single scattered photons only, and denoting the fluence at scattering energy E as $\Psi(E)$, Compton scattering kinematics provides the following formulas,

$$E = \frac{E_0}{1+\alpha(1-\cos\theta)}, \tag{1}$$

$$\begin{aligned}\Psi(E) = {} & \frac{N_0}{|\boldsymbol{B}-\boldsymbol{A}|^2} f_i(\boldsymbol{B}-\boldsymbol{A};E_0)P(E_0;E)\rho(\boldsymbol{B}) \\ & \times \frac{\Delta A}{|\boldsymbol{C}-\boldsymbol{B}|^2} f_o(\boldsymbol{C}-\boldsymbol{B};E)k(E),\end{aligned} \tag{2}$$

where E_0 and E are the energy of the incident photons and the energy of the scattered photons, respectively, θ is the angle of scattering, α is the ratio of E_0 to the energy corresponding to the rest mass of the electron, $|\boldsymbol{B}-\boldsymbol{A}|^2$ is the square of the distance between the source and the scattered point, f_i and f_o are the attenuations for the incident and scattered pathways, respectively, $\rho(\boldsymbol{B})$ is the electron density of the scattered point, P is the probability of Compton scattering from E_0 to E, $|\boldsymbol{C}-\boldsymbol{B}|^2$ is the square of the distance between the scattered point and the detector, ΔA is the area of the detector aperture and $k(E)$ is the detector efficiency evaluated at energy E. From Klein–Nishina formula, P is given by

$$\begin{aligned}P(E_0;E) = {} & \frac{r_{\mathrm{e}}^2}{2}\Big(\frac{E_0}{E}+\frac{E}{E_0}-\sin^2\theta\Big)\Big(\frac{E}{E_0}\Big)^2 \\ = {} & \frac{r_{\mathrm{e}}^2}{2}\Big[\cos^2\theta+\alpha(1-\cos\theta) \\ & +\frac{1}{1+\alpha(1-\cos\theta)}\Big] \\ & \times\Big[\frac{1}{1+\alpha(1-\cos\theta)}\Big]^2,\end{aligned} \tag{3}$$

where r_{e} is the classical radius of the electron.

In Compton scattering tomography, the source is usually a γ source with high energy. The contribution of the photoelectric effect to photon attenuation is small compared with that of Compton scattering, so the photoelectric effect is negligible. f_i and f_o can be given by

$$f_i(E_0) = \exp\Big[-\int_{\boldsymbol{A}}^{\boldsymbol{B}} \rho(l)\times\sigma(E_0)\,\mathrm{d}l\Big], \tag{4}$$

$$f_o(E) = \exp\Big[-\int_{\boldsymbol{B}}^{\boldsymbol{C}} \rho(l)\times\sigma(E)\,\mathrm{d}l\Big], \tag{5}$$

where $\sigma(E_0)$ and $\sigma(E_i)$ are the attenuation coefficients of the incident beam and the scattered beam, respectively, $\rho(l)$ is the electron density at position l along the radiation path.

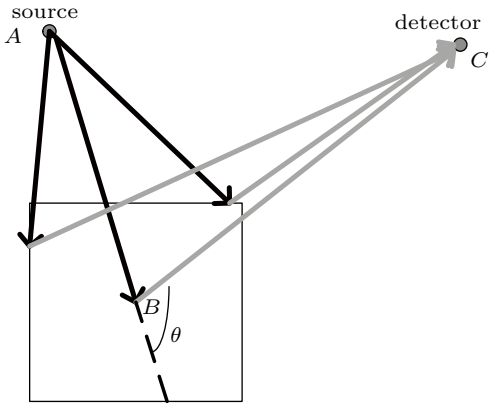


Fig. 1. The Compton scattering imaging system model.

If the object is made into a square grid of $N\times N$ pixels, the detected spectrum is segmented into M

discrete energy regions, with respectively E_i ($i = 1, 2, \ldots M$), then expression (2) can be expressed as

$$\Psi(E_i) = \sum_{j}^{N^2} a_{ij}\rho_j \tag{6}$$

with

$$a_{ij} = \delta_{ij}\frac{N_0}{|B-A|^2} f_i(B-A;E_0)P(E_0;E_i) \times \frac{\Delta A}{|C-B|^2} f_o(C-B;E_i)k(E_i), \tag{7}$$

where the subscript j refers to the j-th pixel, δ_{ij} is a delta function whose value is equal to one when the scattered photons from pixel j contribute to the energy spectrum E_i of the detector, otherwise it is set to be zero. In the matrix notation, expression (6) can be written as

$$\boldsymbol{\Psi} = \boldsymbol{A}(\boldsymbol{\rho})\boldsymbol{\rho}, \tag{8}$$

where matrix $\boldsymbol{A}$ is called the system matrix, which is the forward mapping of the electron densities to the measurements. This is for a single detector element, then, other elements will just add similar rows to the matrix.

From expression (1), we can obtain the relationship between the scattered angle and energy of the scattered photons, which is shown in Fig. 2. In Compton backscatter imaging, the ray source and detectors are located on the same side of the object, so many of the scattered angles are greater than 90°, and the energies of scattered photons change slowly. This means that photons collected by the detector are from a narrow range of the energy spectrum. The energy spectrum range and the energy bin determine the number of measurements, so only a few measurements can be obtained in Compton backscatter imaging.

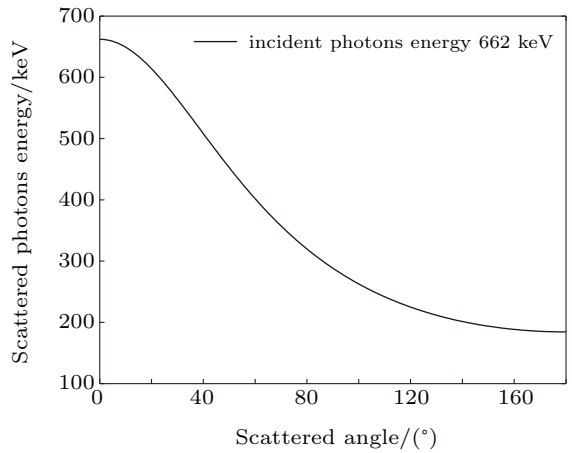


Fig. 2. Relationship between scattered angle and the energy of scattered photons.

3. Compton scattering image reconstruction by TV minimization

The reconstruction problem of Compton scattering imaging is an inverse problem to solve electron densities from the nonlinear equation (8). Generally, the process of solving this inverse problem is to estimate a set of electron densities that accord with the measured data best. The unweighted least-square solution that is obtained from a minimization of the residual between the measurements and its model predictions, has maximum fidelity to the measured data. When the measured data are contaminated by noise, the unweighted least-square solution has maximum fidelity to the noise as well, so this solution is not what we want.

To deal with an ill-posed problem, we can add prior knowledge about the solution to stabilize it. The underlying image function of a medical image is often almost a piecewise constant, so the gradient of an image is often sparse. Using this prior knowledge about the solution, we introduce the TV minimization objective function, and then the reconstruction problem of Compton scattering imaging can be described as follows:

$$\begin{aligned} &\text{argmin}||\boldsymbol{\rho}||_{\text{TV}} \\ &\text{subject to (s.t.) } \boldsymbol{A}(\boldsymbol{\rho})\boldsymbol{\rho} = \boldsymbol{\Psi}, \end{aligned} \tag{9}$$

where

$$\|\boldsymbol{\rho}\|_{\text{TV}} = \sum_{i,j}\sqrt{(\rho_{i,j}-\rho_{i-1,j})^2 + (\rho_{i,j}-\rho_{i,j-1})^2}, \tag{10}$$

where, $\rho_{i,j}$ is the electron density of position (i, j). Defining $\boldsymbol{B} = \boldsymbol{A}(\boldsymbol{\rho})$, expression (9) can then be expressed as

$$\begin{aligned} &\text{argmin}||\boldsymbol{\rho}||_{\text{TV}} \\ &\text{s.t.} \begin{cases} \boldsymbol{B}\boldsymbol{\rho} = \boldsymbol{\Psi}, \\ \boldsymbol{B} = \boldsymbol{A}(\boldsymbol{\rho}). \end{cases} \end{aligned} \tag{11}$$

In Eq. (11), the problem can divide into two alternate steps:

(i) solving the following sub-problem, $\boldsymbol{\rho}^{(i)}$ is obtained as

$$\begin{aligned} &\arg\min ||\boldsymbol{\rho}||_{\text{TV}} \\ &\text{s.t. } \boldsymbol{B}^{(i-1)}\boldsymbol{\rho} = \boldsymbol{\Psi}; \end{aligned} \tag{12}$$

(ii) calculating the matrix $\boldsymbol{B}^{(i)} = \boldsymbol{A}(\boldsymbol{\rho}^{(i)})$, where the superscript i means the i-th iteration.

We can rewrite Eq. (12) as

$$\arg\min\left\{||\boldsymbol{\rho}||_{\text{TV}} + \frac{1}{2}\mu\cdot\|\boldsymbol{B}\boldsymbol{\theta}-\boldsymbol{\Psi}\|_2^2 \;\middle|\; \boldsymbol{\rho}-\boldsymbol{\theta}=0\right\}. \tag{13}$$

The task of solving problem (13) is to find an $(\boldsymbol{\rho}^*, \boldsymbol{\theta}^*, \boldsymbol{\lambda}^*) \in \Omega$,[25,26] such that

$$\begin{cases} ||\boldsymbol{\rho}||_{\mathrm{TV}} - ||\boldsymbol{\rho}^*||_{\mathrm{TV}} + (\boldsymbol{\rho} - \boldsymbol{\rho}^*)^{\mathrm{T}}(-I\boldsymbol{\lambda}^*) \geq 0, \\ \dfrac{1}{2}\mu \cdot \|\boldsymbol{B\theta} - \boldsymbol{\Psi}\|_2^2 - \dfrac{1}{2}\mu \cdot \|\boldsymbol{B\theta}^* - \boldsymbol{\Psi}\|_2^2 + (\boldsymbol{\theta} - \boldsymbol{\theta}^*)^{\mathrm{T}}(I\boldsymbol{\lambda}^*) \geq 0, \quad \forall(\boldsymbol{\rho}, \boldsymbol{\theta}, \boldsymbol{\lambda}) \in \Omega, \\ (\boldsymbol{\lambda} - \boldsymbol{\lambda}^*)^{\mathrm{T}}(\boldsymbol{\rho}^* - \boldsymbol{\theta}^*) \geq 0, \end{cases} \tag{14}$$

where $\Omega = X \times Y \times \mathbb{R}^n$, $X, Y \subset \mathbb{R}^n$ are given closed convex sets.

For given $(\boldsymbol{\theta}, \boldsymbol{\lambda})$, $\boldsymbol{\rho}^{k+1}$ is the solution of the following problem (i.e. Eq. (15)):

$$\boldsymbol{\rho}^{k+1} = \arg\min\Big\{||\boldsymbol{\rho}||_{\mathrm{TV}} - (\boldsymbol{\lambda}^k)^{\mathrm{T}}(\boldsymbol{\rho} - \boldsymbol{\theta}^k) + \frac{1}{2}\beta \cdot \|\boldsymbol{\rho} - \boldsymbol{\theta}^k\|_2^2 | \boldsymbol{\rho} \in X\Big\}. \tag{15}$$

Use $\boldsymbol{\lambda}^k$ and the obtained $\boldsymbol{\rho}^{k+1}$, $\boldsymbol{\theta}^{k+1}$ is the solution of the following problem (i.e. Eq. (16)):

$$\boldsymbol{\theta}^{k+1} = \arg\min\Big\{\frac{1}{2}\mu \cdot \|\boldsymbol{B\theta} - \boldsymbol{\Psi}\|_2^2 - (\boldsymbol{\lambda}^k)^{\mathrm{T}}(\boldsymbol{\rho}^{k+1} - \boldsymbol{\theta}) + \frac{1}{2}\beta \cdot \|\boldsymbol{\rho}^{k+1} - \boldsymbol{\theta}\|_2^2 | \boldsymbol{\theta} \in Y\Big\}, \tag{16}$$

$$\boldsymbol{\lambda}^{k+1} = \boldsymbol{\lambda}^k - \beta(\boldsymbol{\rho}^{k+1} - \boldsymbol{\theta}^{k+1}). \tag{17}$$

The sub-problems (15) and (16) are separately solved. The method of solving these two problems can be found in Ref. [25].

4. Numerical simulations

To demonstrate this new algorithm for Compton scattering image reconstruction, the proposed algorithm is compared with the unweighted least-square method and the EM-ML method. We provide in Fig. 3 the schematic plot of the Compton backscatter imaging system model used in this simulation. In this model, the source is collimated as a fan beam, the energy of the incident photons is 662 keV, and two detector arrays are symmetrically located around the incident beam. The distance between the two neighbouring detectors is 20 mm, the size of detector is 2 mm×2 mm, and the vertical and horizontal distances between the source and the nearest detector cell are 100 mm and 0 mm, respectively. The horizontal and vertical distances between the source and the centre of the object are 64 mm and 0 mm, respectively, and the object is a 32×32 Shepp–Logan phantom, so the number of unknown electron densities is 1024.

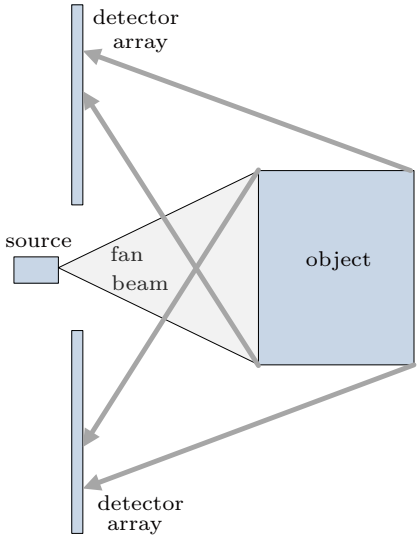


Fig. 3. System model used in this paper.

The measured data are generated by Eq. (8). In order to perform simulations in the presence of noise, we incorporate an additive noise component dependent on the projections into the measurements,[27] such that

$$\boldsymbol{\Psi}' = \boldsymbol{\Psi} + N(\mu, \sigma^2) * \boldsymbol{\Psi}, \tag{18}$$

where $\boldsymbol{\Psi}'$ means the measurements including noise, $N(\mu, \sigma^2)$ means a Gaussian function which has a mean μ and a variance σ^2. In this work, $\mu = 0$ and $\sigma = 0.01$.

Image quality is evaluated by the root mean square error (RMSE), which is defined as

$$\mathrm{RMSE} = \sqrt{\frac{(\boldsymbol{\rho}' - \boldsymbol{\rho})^{\mathrm{T}}(\boldsymbol{\rho}' - \boldsymbol{\rho})}{N}}, \tag{19}$$

where $\boldsymbol{\rho}'$ and $\boldsymbol{\rho}$ (column vector) are the electron densities of the real image and the electron densities of the reconstructed image, respectively, and N is the total number of pixels in the image.

In this study, the detector arrays are arranged at the same side of the source, so the imaging situation is worse because detectors can collect only the backscatter photons. The photons collected by detectors have a narrow energy range, so the measurements are fewer.

For the first step, we use 25 detectors for each detector array, so the total number of detectors is 50. Reconstruction results with and without noise, when the energy bin is set to 2 keV, are shown in Figs. 4 and 5, respectively. We define k as the number of global iterations.

For Fig. 4, when we use fifty detectors and set the energy bin at 2 keV, the total number of measurements is greater than the unknown density, and all of the methods can reconstruct the image with a low error in the absence of noise. The TV minimization algorithm is slightly better. After adding noise to the measurements, the result of the TV minimization algorithm shows more advantages than the other two methods as shown in Fig. 5.

For the second step, we use 20 detectors for each detector array, so the total number of detectors is 40. Reconstruction results without and with noise when the energy bin is set at 2 keV are shown in Figs. 6 and 7, respectively.

In Figs. 6 and 7, the total number of measurements is less than the unknown density. Even without noise, the image quality of the unweighted least-square method and EM-ML method becomes worse, but the TV minimization algorithm appears to lead to more accurate reconstructed images. In the presence of noise, the proposed algorithm is obviously better than the other two methods.

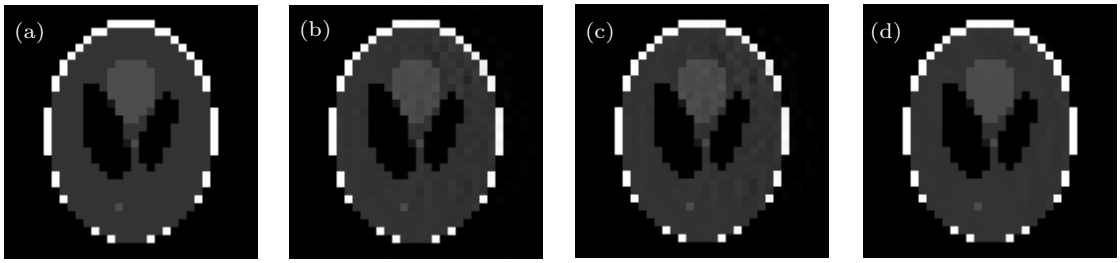


Fig. 4. Reconstruction results without noise for the unweighted least-square method, the EM-ML method, and the TV minimization algorithm when the number of detectors is 50. (a) The Shepp–Logan phantom. (b) The result of the unweighted least-square method, $k = 20$, RMSE = 0.0087. (c) The result of the EM-ML method, $k = 20$, RMSE = 0.0047. (d) The result of the TV minimization algorithm, $k = 20$, RMSE = 0.0032.

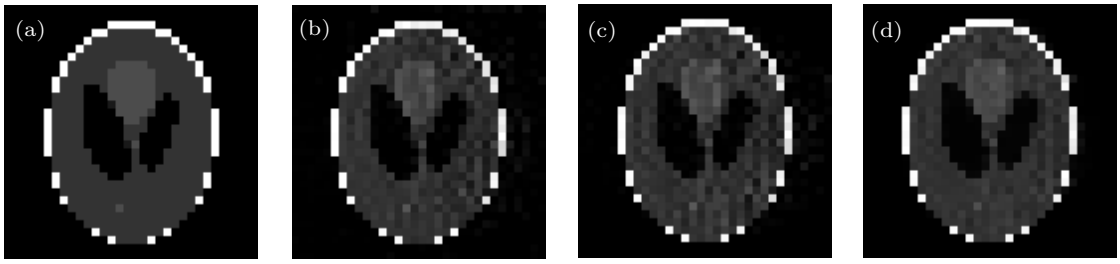


Fig. 5. Reconstruction results with noise for the unweighted least-square method, the EM-ML method, and the TV minimization algorithm when the number of detectors is 50. (a) The Shepp–Logan phantom. (b) The result of the unweighted least-square method, $k = 20$, RMSE = 0.03. (c) The result of the EM-ML method, $k = 7$, RMSE = 0.0321. (d) The result of the TV minimization method, $k = 7$, RMSE = 0.0208.

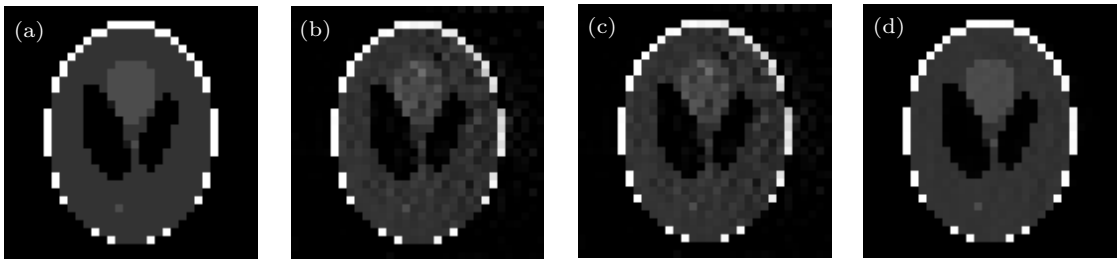


Fig. 6. Reconstruction results without noise for the unweighted least-square method, the EM-ML method, and the TV minimization algorithm when the number of detectors is 40. (a) The Shepp–Logan phantom. (b) Result of the unweighted least-square method, $k = 20$, RMSE = 0.0315. (c) Result of the EM-ML method, $k = 20$, RMSE = 0.0214. (d) Result of the TV minimization algorithm, $k = 20$, RMSE = 0.0062.

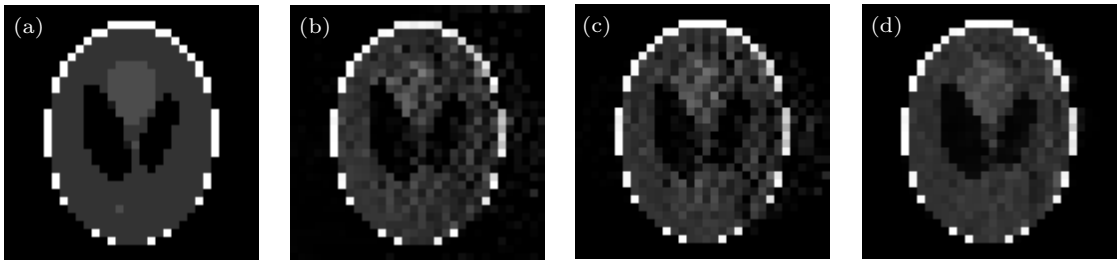


Fig. 7. Reconstruction results with noise for the unweighted least-square method, the EM-ML method, and the TV minimization algorithm when the number of detectors is 40. (a) The Shepp–Logan phantom. (b) Result of the unweighted least-square method, $k = 20$, RMSE = 0.0556. (c) Result of the EM-ML method, $k = 7$, RMSE = 0.0544. (d) Result of the TV minimization algorithm, $k = 7$, RMSE = 0.0282.

For the last step, we use 15 detectors for each detector array, so the total number of detectors is 30. The number of measurements is fewer than that at the second step. Reconstruction results without noise, when the energy bin is set at 2 keV, are shown in Fig. 8.

In Fig. 8, because the total number of measurements is less than the number of unknown electron densities, the image qualities of the unweighted least-square method and the EM-ML method become worse more rapidly than those at the second step, but the TV minimization algorithm gives a more accurate image.

Figure 9 shows the accuracies for different solution methods. We can see that the TV minimization algorithm is obviously more accurate.

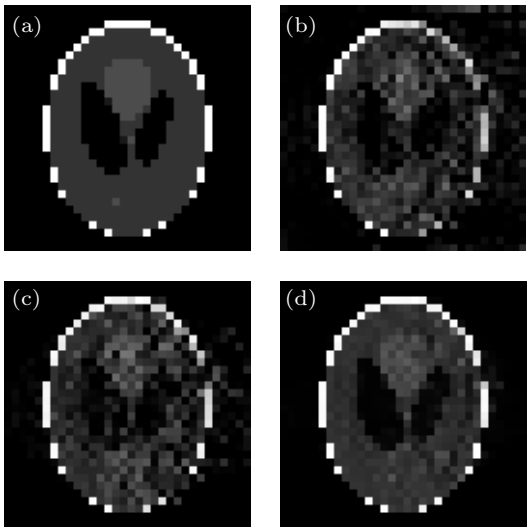


Fig. 8. Reconstruction results without noise for the unweighted least-square method, the EM-ML method, and the TV minimization algorithm when the number of detectors is 30. (a) The Shepp–Logan phantom. (b) Result of the unweighted least-square method, $k = 20$, RMSE = 0.0903. (c) Result of the EM-ML method, $k = 20$, RMSE = 0.0744. (d) Result of the TV minimization algorithm, $k = 20$, RMSE = 0.0292.

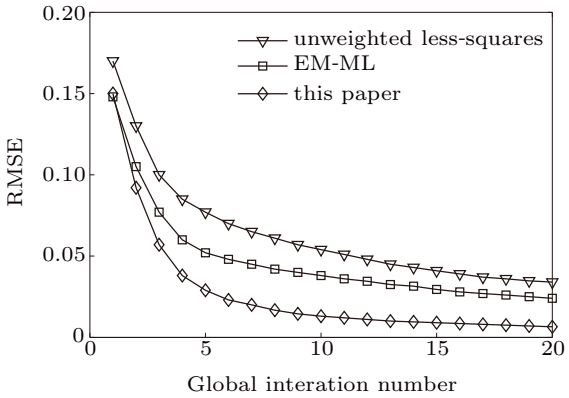


Fig. 9. Comparison among density errors for different reconstruction procedures.

5. Conclusion

Introducing an objective function of TV minimization, a new image reconstruction algorithm is proposed in this paper. This algorithm seeks an image which has the minimum TV amongst all images that match the measured data. The simulated results show that the proposed algorithm can reduce reconstruction error and improve image quality, especially when the number of measurements is fewer.

References

[1] Jia P X, Zhang F, Yan B and Bao S L 2010 *Chin. Phys.* B **19** 087802
[2] Luo Z Y, Yang X Q, Meng Y Z and Deng Y 2010 *Acta Phys. Sin.* **59** 8237 (in Chinese)
[3] Lale P G 1959 *Phys. Med. Biol.* **4** 159
[4] Battista J J and Bronskill M J 1981 *Phys. Med. Biol.* **26** 81
[5] Farmer F T and Collins M P 1971 *Phys. Med. Biol.* **16** 577
[6] Harding G and Harding E 2010 *Appl. Rad. Iso.* **68** 993
[7] Andy C Ho 1994 *Quantification of Gamma-Ray Compton-Scatter Nondestructive Testing*, MS dissertation, New Brunswick, University of New Brunswick
[8] Tang S and Hussein E M A 2004 *Appl. Rad. Iso.* **61** 3

[9] Khettabi F E, Yarr I and Hussein E M A 2003 *Phys. Med. Biol.* **48** 3445
[10] van Uytven E, Pistorius S and Gordon R 2008 *Phys. Med. Biol.* **53** 5445
[11] van Uytven E, Pistorius S and Gordon R 2007 *Med. Phys.* **34** 256
[12] Kondic N N, Jacobs A M and Ebert D 1983 *Proc. of the 2nd International Topical Meeting on Nuclear Reactor Thermal-Hydraulics,* January 11–14, 1983, Santa Barbara, USA, p. 1443
[13] Hussein E M A, Meneley D A and Banerjee S 1986 *Nucl. Sci. Eng.* **92** 341
[14] Arendtsz N V and Hussein E M A 1993 *Mathematical Methods in Medical Imaging* II **2035** 230
[15] Arendtsz N V and Hussein E M A 1995 *IEEE Trans. Nucl. Sci.* **42** 2155
[16] Candes E, Romberg J and Tao T 2006 *IEEE Trans. Inf. Theory* **52** 489
[17] Sidky E Y and Pan X 2006 *Nuclear Science Symposium Conference Record*, October 29–November 1, 2006, San Diego, CA, p. 2904
[18] Sidky E Y, Kao C M and Pan X 2006 *Nuclear Science Symposium Conference Record,* San Diego, CA, October 29–November 1, 2006, USA, p. 2296
[19] Sidky E Y and Pan X 2008 *Phys. Med. Biol.* **53** 4777
[20] Sidky E Y and Pan X 2009 *Med. Phys.* **36** 4920
[21] Wang L Y, Li L, Yan B, Jiang C S, Wang H Y and Bao S L 2010 *Chin. Phys.* B **19** 088106
[22] Ritschl L, Bergner F, Fleischmann C and Kachelrie M 2011 *Phys. Med. Biol.* **56** 1545
[23] Persson M, Bone D and Elmqvist H 2011 *Phys. Med. Biol.* **46** 853
[24] Lu X, Sun Y and Yuan Y 2011 *Pattern Recognition* **44** 2427
[25] Li C B 2009 *An Efficient Algorithm for Total Variation Regularization with Applications to the Single Pixel Camera and Compressive Sensing*, MS dissertation, Houston, Rice University
[26] Chen C H, He B S and Yuan X M 2012 *IMA J. Numer. Anal.* **32** 227
[27] Wang Y and Lu W 1992 *Singal Processing* **26** 17